Zinc oxide's hierarchical nanostructure and its photocatalytic properties

Kanjwal, Muzafar Ahmed; Sheikh, Faheem A.; Barakat, Nasser A. M.; Li, Xiaoqiang; Kim, Hak Yong; Chronakis, Ioannis S.

Published in:
Applied Surface Science

Link to article, DOI:
10.1016/j.apsusc.2011.12.008

Publication date:
2012

Title: Zinc oxide's hierarchical nanostructure and its photocatalytic properties

Authors: Muzafar A. Kanjwal, Faheem A. Sheikh, Nasser A.M. Barakat, Xiaoqiang Li, Hak Yong Kim, Ioannis S. Chronakis

PII: S0169-4332(11)01899-X
DOI: doi:10.1016/j.apsusc.2011.12.008
Reference: APSUSC 22814

To appear in: *APSUSC*

Received date: 21-4-2011
Revised date: 29-11-2011
Accepted date: 3-12-2011

Please cite this article as: M.A. Kanjwal, F.A. Sheikh, N.A.M. Barakat, X. Li, H.Y.K. </sup>Ioannis S. Chronakis, Zinc oxide's hierarchical nanostructure and its photocatalytic properties, *Applied Surface Science* (2010), doi:10.1016/j.apsusc.2011.12.008

Research highlights.

- The nanofibers from colloidal solution of mixture containing Zinc acetate, poly vinyl alcohol, and zinc powder, were successfully achieved by electrospinning.
- These nanofibers after calcinations at 500 ^{o}C for 90 minutes, containing the zinc nanoparticles has been exploited as the seeds to grow nanobranches followed by hydrothermal technique.
- The produced hierarchical structure could be utilized in many exciting fields such as dye degradation, photoluminescence etc.

Zinc oxide's hierarchical nanostructure and its photocatalytic properties

Muzafar A. Kanjwal,[a*] Faheem A. Sheikh[c], Nasser A. M. Barakat[b,], Xiaoqiang Li [a], Hak Yong Kim[b,] Ioannis S. Chronakis[a,*]

[a]Technical University of Denmark, DTU Food, Soltofts plads, B 227, 2800 Kgs. Lyngby, Denmark

[c]Department of Chemistry, University of Texas Pan American, Edinburg, TX, 78539, USA

[b]Department of Textile Engineering, Chonbuk National University, Jeonju 561-756, Republic of Korea

Corresponding authors:

Ioannis S. Chronakis

Tel: +45 45 25 2613

Fax: +45 45 939600

E-mail address*:* ***ioach@food.dtu.dk***

Muzafar Ahmad Kanjwal

E-mail address*:* ***muka@food.dtu.dk***

Tel: +45 50 187467

Fax: +45 45 939600

Abstract

In this study, a new hierarchical nanostructure that consists of zinc oxide (ZnO) was produced by the electrospinning process followed by a hydrothermal technique. First, electrospinning of a colloidal solution that consisted of zinc nanoparticles, zinc acetate dihydrate and poly(vinyl alcohol) was performed to produce polymeric nanofibers embedding solid nanoparticles. Calcination of the obtained electrospun nanofiber mats in air at 500 ^{o}C for 90 minutes produced pure ZnO nanofibers with rough surfaces. The rough surface strongly enhanced outgrowing of ZnO nanobranches when a specific hydrothermal technique was used. Methylene blue dihydrate was used to check the photocatalytic ability of the produced nanostructures. The results indicated that the hierarchical nanostructure had a better performance than the other form.

Keywords: Zinc oxide, Zinc nanoparticles, Electrospinning, Hydrothermal, Methylene Blue.

1. Introduction

During the past 100 years, zinc oxide (ZnO) has had extensive commercial use, with thousands of tons produced each year [1]. The remarkable properties of ZnO are its high exciton binding energy of 60 mV at room temperature and its wide, direct band gap of 3.37 eV [2]. ZnO is a typical electroceramic material and has promising applications in ultraviolet light emitting diodes, functional devices, dye-sensitized solar cells, chemical sensors, piezoelectric materials and transparent conductors [3-6]; in addition, it is inexpensive, nontoxic, and chemically stable. The optical and electronic properties of ZnO nanostructures are largely dependent on their composition, crystal quality, structural defects, dimensions and shape [7,8]. It is worth mentioning that a one-dimensional ZnO nanostructure with an effective morphology has a significant potential in efficient construction and performance of nanoscale devices due to the quantum restriction of charge carriers in small extent [9-12]. Among the one-dimensional nanostructures, nanofibers are particularly interesting because of their long axial ratio, which has a distinct impact on the physical and chemical characteristics. ZnO nanofibers have already been reported and have been found to have good properties [13]; electrospinning is the most widely used technique to produce pristine ZnO or ZnO-based nanofibers.

To further improve the physiochemical properties of functional materials, researchers have turned to the synthesis of complex architectures with controlled alignment, sizes, shapes, and compositions that are based on one-dimensional structures. These new morphologies are of great interest because their hierarchical structures may provide opportunities to obtain new phenomena and novel properties. Many functional materials have been reported, such as the heterogeneous structures of ZnO/SnO_2 via a

thermal evaporation of Zn powders [14], ZnO/In_2O_3 by a vapor transport and condensation technique [15], and SnO_2/Fe_2O_3 through a hydrothermal method [16,17]. Homogeneous structures of SnO_2/SnO_2 have also been produced by a multistep thermal vapor deposition procedure [18], while nanowire–nanoribbon junction arrays of ZnO have been produced through a vapor–liquid–solid process [19]. In this field, we recently introduced **Co_3O_4**-ZnO hierarchical structure, which performed well when utilized as catalyst in degradation of rhodamine B dye [20]. Accordingly, the main aim of this work is to introduce ZnO in a new hierarchical structure and to study the effect of this new morphology on the photocatalytic properties. The target structure is nanofibers that emanate branches.

Electrospinning is an electrostatic, nonmechanical method; in comparison to conventional spinning techniques, it easily creates solid fibers in the nanometer to micrometer range [21]. As aforementioned, ZnO nanofibers created by the electrospinning process have already been introduced; investigations into the surface morphology of the nanofibers showed a smooth surface, which was also observed in this study. Outgrowing branches around a nanofiber with a smooth surface is not feasible because the cohesion will be feeble. However, a rough surface makes the outgrowing process easier with a strong product. Consequently, the product can be confidently exploited in various applications. Recently, we reported electrospinning of colloidal solutions as a novel technique to give wide latitude to the electospinning process, while producing a new class of electrospun materials. [22]. This technique has been utilized to produce ZnO nanofibers with a rough surface. Typically, a colloidal solution that was composed of zinc acetate dehydrate, poly-vinyl alcohol (PVA) and zinc nanoparticles

(ZnNPs) was electrospun; then, calcination of the obtained electrospun mats resulted in ZnO nanofibers with a rough surface. It is noteworthy to mention that using a (ZnNPs) free solution produced a smooth surface on the ZnO nanofibers [23]. Nanobranches from ZnO have been successfully outgrown from the prepared nanofibers by a hydrothermal treatment process in the presence of zinc nitrate and bis-hexamethylene triamine.

The obtained hierarchical nanostructure and the individual constituent were then separately used as photocatalysts for degradation of methylene blue dye (MB). The hierarchical nanostructure showed better results than its ingredient.

2. Experimental section

2.1 Materials

Zinc nano powder and bis-hexamethylene triamine were obtained from Aldrich, USA. Zinc nitrate hexahydrate, MB dihydrate (95.0 assay) and zinc acetate dehydrate were obtained from Showa, Japan. (PVA) with a molecular weight (MW) of 65,000 g/mol was obtained from Dong Yang Chem, South Korea. All of these materials were used without any further purification. Distilled water was used as a solvent.

2.2 Characterization

The surface morphology of the nanofibers was studied with a JEOL JSM-5900 scanning electron microscope, JEOL Ltd, Japan. The phase and crystallinity were characterized by using a Rigaku X-ray diffractometer (Rigaku, Japan) with Cu Kα (λ = 1.54056 A^o) radiation over the 2θ range of angles from 20 to 90^o. Before TEM analysis, the powdered samples were dispersed in methanol by sonication; then, they were placed and dried by normal evaporation. High-resolution images and selected area electron

diffraction pattern were observed with a JEOL JEM 2010 transmission electron microscope (TEM) that operated at 200 kV, JEOL, Japan. The surface composition was detected with an X-ray photoelectron spectroscopy analysis (XPS, AXIS-NOVA, Kratos Analytical, UK) with the following conditions: base pressure of 6.5 x 10^{-9} Torr, resolution (pass energy) of 20 eV and scan step of 0.05 eV/step. The concentration of the dyes and the optical properties was studied by using a HP 8453 UV Visible Spectroscopy System; the spectra were analyzed with HP ChemiStation software 5890 series.

2.3 Electrospinning set-up and development of ZnO nanobranches

To electrospin the colloidal solutions that contained zinc acetate (ZnAc), PVA, and ZnNPs, the following stepwise methodology was adopted. First, PVA (14 wt%) solution was made by dissolving PVA granules in distilled water at room temperature with vigorous stirring for 24 h. Then, 1 g of ZnAc was dissolved in 5 g of distilled water and mixed with the PVA solution. To this solution, 0.1 g of zinc powder was added. The resultant colloidal solution was stirred for 10 min. A high-voltage power supply (CPS-60 K02V1, Chungpa EMT, Republic of Korea) was used as the source of the electric field. The colloidal solution was supplied through a plastic syringe attached to a capillary tip. A positive electrode (anode) connected to a copper pin was inserted into the colloidal solution, and a negative electrode (cathode) was attached to a metallic collector that was covered with a polyethylene sheet. The solution was briefly electrospun at 20 kV and a 15-cm working distance (the distance between the needle tip and the collector). The formed nanofiber mats were initially dried for 24 h at 80 ^{o}C under vacuum in the

presence of P_2O_5 and then calcined in air at 500 ^oC for 90 minutes, with a heating rate of 5 ^oC/min.

According to previous studies [24,25], pure ZnO nanostructures can be obtained by using a hydrothermal treatment of aqueous solution that contains Bis-hexamethylene triamine and zinc nitrate hexahydrate. Therefore, ZnO nanobranches were outgrown from the prepared ZnO nanofibers by using the same strategy. The process was carried out in a stainless steel reactor with a 15-cm height and 7-cm diameter. The experiment was conducted as follows: typically, 1 g of bis-hexamethylene triamine was dissolved in 50 g of water. In another bottle, 1.5 g of zinc nitrate hexahydrate was dissolved in 50 g of water. These solutions were mixed and 10 mg of the calcined nanofibers was added; the slurry was then vigorously stirred for a long time and placed in a teflon crucible at the bottom of the reactor. The sealed reactor was maintained at 150 ^oC for 1 h and then naturally cooled to room temperature. The obtained product was filtered off, washed several times with distilled water, and dried at 60 ^oC for 12 h for further analysis.

3. Results and discussions

Figures 1A and B show SEM images of the dried electrospun nanofiber mats that were prepared from ZnAc/PVA at low and high magnifications. As can be clearly seen, smooth and continuous nanofibers formed after electrospinning of the prepared sol-gel. Figures 1C and 1D show SEM images of the dried (Zn NPs)/(ZnAc/PVA) colloid at low and high magnifications. As can be concluded from Fig. 1C and 1D, the addition of (ZnNPs) did not affect the morphology of the nanofibers; the regular shape and absence of beads are observable from the SEM images.

Calcination of both formulations resulted in a decrease in the average diameter of the calcined nanofibers in comparison to the electrospun ones as can be observed from Fig. 2, which shows SEM images of the nanofibers after calcination for both formulations held at 500 ^{o}C for 90 minutes. A decreasing nanofiber diameter in both formulations can be explained by the removal of the polymer by calcination at high temperature. In Fig. 2, the addition of (ZnNP) does not affect the nanofibrous shape in general (Fig. 2C and 2D); however, there is a distinct effect on the surface of the produced nanofibers. Fig. 2B and D show high magnification SEM images of the calcined powder that was obtained from ZnAc/PVA and Zn NPs/ZnAc/PVA, respectively; there is an observable difference between the surfaces in the two formulations. In the case of the nanofibers obtained from calcination of (ZnAc/PVA), the surface of the nanofibers was relatively smooth and no imperfections were observed, while addition of (ZnNP) to the electrospun solution led to a rough surface.

To properly investigate the nature of the surfaces, atomic force microscopy (AFM) was used, and the results are shown in Fig. 3. As shown in the two and three dimensional images, the surface of the nanofibers that were obtained from the ZnAc/PVA mother solution is smooth (Fig. 3A and 3B). However, a clearly rough surface was generated due to the addition of (ZnNP) (Fig 3B and 3C).

Transmission electron microscopy (TEM) can be used to differentiate between the crystalline and amorphous structures. Moreover, it gives reliable information about the surface morphology. Structural characterization of the nanofibers that were prepared by calcination of (ZnAc) and (PVA) is shown in Fig. 4A and 4B at high and low magnification. It can be concluded from Fig. 4A that the surface is smooth with clear

borders; the SAED pattern at (inset) indicates good crystallinity. Figures 4C and 4D show the high and low magnification TEM images, respectively, of the calcined nanofibers obtained from the solution that contained the (ZnNPs); these images show that the surface is not smooth and the borders are not clear. This finding supports the AFM results, which reveal the surface roughness of the nanofibers obtained from the electrospun solution that contained (ZnNPs). The inset in Fig. 4D, which represents the corresponding SAED pattern, indicates good crystallinity as in the Zn NP-free case.

Preparation of ZnO nanorods by a hydrothermal technique is a well-known process previously reported by some researchers [24,25]. In this study, the hydrothermal technique was utilized to outgrow ZnO around the prepared nanofibers. The hydrothermal technique was carried out under the same conditions for both formulations. Figures 5A and 5B represent SEM images of nanofibers that were obtained from the NP-free solution and that underwent the hydrothermal process. The absence of outgrowths from the nanofibers can be clearly seen. However, as shown in Fig. 5C and 5D, small outgrowths can be seen around the nanofibers that were obtained from the (ZnNPs) containing solution due to the hydrothermal treatment process. To observe these nail-like structures, we used a FE-SEM analysis to obtain more precise information. Figure 5E shows the resulting FE-SEM images. According to many previously reported studies [24,25], the newly formed branches can be assessed as ZnO. To practically investigate the effect of addition of ZnNPs, the surface area of **all formulations has** been measured by using Brunauer-Emmett-Teller (BET) technique (ASAP 2010 micromeritics, USA). The average surface area of the ZnNPs-free nanofibers was about 20.4409 m^2/g, while, it was 34.2201 m^2/g for the nanofibers containing ZnNPs, **similarly 49.7701 m^2/g for**

hydrothermal product. As can be concluded from these results, the high surface area of the ZnNPs containing nanofibers enhances the photocatalytic activity.

The crystal structures of the calcined nanofibers and powder obtained from the hydrothermal process were examined by XRD (see Fig, 6); spectra A refers to the calcined nanofibers and represents pure ZnO material. The apparent peaks at 2θ values of 31.66, 34.22, 36.25, 47.86, 56.51, 62.66, 67.37, 67.92 and 69.266^{o} correspond to the crystal planes of (100), (002), (101), (102), (110), (103), (200), (112), and (201), which confirms the formation of pure ZnO (JCPDS card No 36-1451). **The crystallite size of hydrothermal product was estimated with well-known scherrer equation [26] with FWHM of X-ray diffraction pattern, and the value of peak positions were shown in a Table 1.**

$$D = 0.9\lambda / \beta\cos\theta.$$

where λ corresponds to wavelength of X-ray radiation source, β is full-width at half-maximum in [FWHM] radians, θ refers to Bragg's diffraction angle. The calculation was measured with the help of Gaussian Lorentzian fitting Program. The average value of particle sizes is ~26 nm.

It is noteworthy to mention that the addition of Zn NPs to the electrospun solution did not affect the XRD results because the spectra were the same in both cases. Spectra B from the as obtained powder subjected to the hydrothermal process have the same peaks, while the absence of other peaks indicates that the branches of the produced nanofibers only consisted of ZnO. To simplify, in Fig. 6, we have marked the peaks that

correspond to zinc dioxide as Z. Overall, the results confirm the formation of ZnO nanofibers.

Figure 7A and 7B show low and high magnification TEM images, respectively, for the nanostructure that was obtained after the hydrothermal process. As shown in this figure, outgrowths were obtained everywhere in the main nanofibers, which is consistent with the density, morphology, and dimension obtained in the SEM and FE-SEM images. Figure 7C shows a HRTEM image for the marked nanobranch in the produced main nanobranched ZnO nanofiber; the existence of parallel atomic planes reveals excellent crystallinity for the outgrowing branches. The inverse fast Fourier transformation (FFT) image at the top inset of Fig. 7C also confirms good crystallinity, which is in accordance with HRTEM.

The proposed mechanism by which ZnO nanobranches were developed from the ZnO nanofibers is shown in scheme 1. The colloidal solution after electrospinning results in the formation of ZnO/PVA nanofibers containing ZnNPs. The subsequent calcination of these nanofibers results in the oxidation of ZnNPs to ZnO NPs. These nanofibers when subjected to hydrothermal process as mentioned above results in the formation of ZnO nanobranches that surrounds ZnO nanofibers.

To investigate the oxidation states as well as possible changes to the binding energies of the as-prepared hydrothermal product, and to support the XRD data an X-ray photoelectron spectroscopy (XPS) analysis was performed. The samples for XPS were supported by carbon cloth electrodes, which are widely used in electrochemical experiments. No heat treatment on the samples was needed. The results are shown in Fig. 8. The peak at 284 eV that corresponds to the C 1s is

understandable, when considering the graphite tape used during the sampling process. The Zn 2p region in ZnO consists of the main 2p3/2 and 2p1/2 spin-orbit components with binding energies of 1020 and 1043 eV, respectively. In addition to 2p, we also observed the 3d, 3p and 3s spin-orbit components for Zn at the binding energy of 10, 88 and 139 eV, respectively [27].

3.1. Photocatalytic properties

To check the photocatalytic degradation of dye, MB was used as blank (without ZnO nanofibers), in the presence of pure ZnO nanofibers and ZnO-ZnO hierarchical nanostructures was carried out in a simple photoreactor. The reactor was made of glass (1000-ml capacity, 23-cm height and 15-cm diameter), covered with alumina foil and equipped with an ultra-violet lamp emitting source at a 365-nm wavelength radiation. The pH of the MB solution at room temperature was 6.9. The initial dye solution and photocatalyst were placed in the reactor and continuously stirred until completely mixed during the photocatalytic reaction. Typically, 100 ml of dye solution (10 ppm, concentration) and 50 mg of catalyst were used. At specific time intervals, a 2-ml sample was withdrawn from the reactor and centrifuged to separate the residual nanofiber catalyst; then, the absorbance intensity was measured at the corresponding wavelength [**28**]. Figure 9 shows the results. In the case of blank, less than 8% of the dye was oxidized even after 3 h. Utilization of the hierarchical nanostructure (hydrothermal product) reveals a significant increase in the degradation rate of this dye. As can be observed in this figure, within 60 min, about 97% of the dye degraded; moreover, the dye was completely eliminated after 75 min. However, in the case of pure ZnO nanofibers,

almost 20% of the dye was oxidized after 60 min and all of the dye could not be eliminated from solution even after 3 h.

4. Conclusion

In summary, electrospinning of ZnNP/ZnAc/PVA colloid can be successfully achieved. Addition of (ZnNPs) leads to the production of pure ZnO nanofibers with a rough surface. The rough surface strongly enhances outgrowing of ZnO nanobranches around the prepared nanofibers when a specific hydrothermal technique is used. Utilizing the synthesized hierarchical nanostructure to decay MB dye produces interesting results because the MB dye solution became colorless after 60 min. The results strongly recommend exploiting the synthesized ZnO-ZnO nanofibers as a super active photocatalyst.

Acknowledgement

This work was supported by a grant of the Korean Ministry of Education, Science and Technology (The Regional Core Research Program/Center for Healthcare Technology & Development, Chonbuk National University, Jeonju 561-756, Republic of Korea) and Woongjin Chemical Co., Suwon 443-270, Republic of Korea. We thank Mr. T. S. Bae KBSI of the Jeonju branch and Mr. Jong-Gyun Kang of the Centre for University Research Facility for providing the facilities to do FESEM and TEM images, respectively.

References

[1]. R.B. Peterson, C.L. Fields, A.B. Gregg, Epitaxial Chemical Deposition of ZnO Nanocolumns from NaOH Solutions, Langmuir, 20 (2004) 5114-5118.

[2]. U. Hiroyuki, Influence of Surfactant Micelles on Morphology and Photoluminescence of Zinc Oxide Nanorods Prepared by One-Step Chemical Synthesis in Aqueous Solution, J. Phys. Chem. C., 111 (2007) 9060-9065.

[3]. H. Kind, H.Q. Yan, B. Messer, M. Law, P.D. Yang, Nanowire Ultraviolet Photodetectors and Optical Switches, AdV. Mater., 14 (2002) 158-160.

[4]. M. Izaki, S. Watase, H. Takahashi, Room-temperature ultraviolet light-emitting zinc oxide micropatterns prepared by low-temperature electrodeposition and photoresist, App. Phys. Lett., 83 (2003) 4930-4932.

[5]. S. Hingorani, V. Pillai, P. Kumar, M.S. Multani, D.O. Shah, Microemulsion mediated synthesis of zinc-oxide nanoparticles for varistor studies, Mater.Res. Bull., 28 (1993) 1303-1310.

[6]. S. Sakohara, M. Ishida, M.A. Anderson, Visible Luminescence and Surface Properties of Nanosized ZnO Colloids, J. Phys. Chem. B 102 (1998) 10169-10175.

[7]. Z. Zhang, S. Liu, S. Chow, M.Y. Han, Modulation of the Morphology of ZnO Nanostructures via Aminolytic Reaction: From Nanorods to Nanosquamas, Langmuir, 22 (2006) 6335-6340.

[8]. F. Ochanda, K. Cho, D. Andala, T.C. Keane, A. Atkinson, W.E. Jones, Synthesis and Optical Properties of Co-Doped ZnO Submicrometer Tubes from Electrospun Fiber Templates, Langmuir, 25 (2009) 7547-7552.

[9]. M.H. Huang, H. Feick, E. Weber, Y. Wu, N. Tran, P. Yang, Catalytic Growth of Zinc Oxide Nanowires by Vapor Transport, Adv. Mater., 13 (2001) 113-116.

[10]. X.Y. Kong, Z.L. Wang, Polar-surface dominated ZnO nanobelts and the electrostatic energy induced nanohelixes, nanosprings and nanospirals, Appl. Phys. Lett., 84 (2004) 975-978.

[11]. W.L. Hughes, Z.L. Wang, Formation of Piezoelectric Single-Crystal Nanorings and Nanobows, J. Am. Chem. Soc., 126 (2004) 6703-6709.

[12]. Z.L. Wang, X.Y. Kong, J.M. Zuo, Induced Growth of Asymmetric Nanocantilever Arrays on Polar Surfaces, Phys. Rev. Lett., 91 (2003) 185502-185505.

[13]. B. Ding, T. Ogawa, J. Kim, K. Fujimoto, S. Shiratori, Fabrication of a super-hydrophobic nanofibrous zinc oxide film surface by electrospinning, Thin Solid Films, 516 (2008) 2495-2501.

[14]. S.H. Sun, G.W. Meng, G.X. Zhang, L.D. Zhang, Controlled Growth and Optical Properties of One-Dimensional ZnO Nanostructures on SnO_2 Nanobelts, Cryst. Growth Des., 7 (2007) 1988-1991.

[15]. J.Y. Lao, J.G. Wen, Z.F. Ren, Hierarchical ZnO Nanostructures, Nano Lett., 2 (2002) 1287-1291.

[16]. H.G. Yang, H.C. Zeng, Synthetic Architectures of $TiO_2/H_2Ti_5O_{11}\cdot H_2O$, $ZnO/H_2Ti_5O_{11}\cdot H_2O$, $ZnO/TiO_2/H_2Ti_5O_{11}\cdot H_2O$, and ZnO/TiO_2 Nanocomposites, J. Am. Chem. Soc., 127 (2005) 270-278.

[17]. D.F. Zhang, L.D. Sun, C.J. Jia, Z.G. Yan, L.P. You, C.H. Yan, Hierarchical Assembly of SnO_2 Nanorod Arrays on α-Fe_2O_3 Nanotubes: A Case of Interfacial Lattice Compatibility, J. Am. Chem. Soc., 127 (2005) 13492-13493.

[18]. S.H. Sun, G.W. Meng, G.X. Zhang, J.P. Masse, L.D. Zhang, Controlled Growth of SnO2 Hierarchical Nanostructures by a Multistep Thermal Vapor Deposition Process, Chem. Eur. J., 13 (2007) 9087-9092.

[19]. P.X. Gao, Z.L. Wang, Self-Assembled Nanowire−Nanoribbon Junction Arrays of ZnO, J. Phys. Chem. B., 106 (2002) 12653-12658.

[20]. M.A. Kanjwal, F.A. Sheikh, N.A.M. Barakat, Ioannis S. Chronakis, H.Y. Kim, Co3O4-ZnO hierarchical nanostructures by electospinning and hydrothermal methods, Appl. Sur. Sci. 257 (2011) 7975-7981.

[21]. D.H. Reneker, A.L. Yarin, S. Koombhongse, Bending instability in electrospinning of nanofibers, J. Appl. Phys., 89 (2001) 3018-3027.

[22]. N.A.M. Barakat, M.F. Abadir, F.A. Sheikh, M.A. Kanjwal, S.J. Park, H.Y. Kim, Polymeric nanofibers containing solid nanoparticles prepared by electrospinning and their applications, Chem. Eng. J., 156 (2010) 487-495.

[23]. Z. Zhang, X. Li, C. Wang, L. Wei, Y. Liu, C. Shao, ZnO Hollow Nanofibers: Fabrication from Facile Single Capillary Electrospinning and Applications in Gas Sensors, J. Phys. Chem. C., 113 (2009) 19397–19403.

[24]. J. Lee, B.S. Kang, B. Hicks, T.F. Chancellor, B.H. Chu, H.T. Wang, B.G. Keselowsky, F. Ren, T.P. Lele, The control of cell adhesion and viability by zinc oxide nanorods, Biomaterials, 29 (2008) 3743-3749.

[25]. M.A. Kanjwal, N.A.M. Barakat, F.A. Sheikh, S.J. Park, H.Y. Kim, Photocatalytic activity of ZnO-TiO_2 Hierarchical nanostructure prepared by combined electrospinning and hydrothermal techniques, Macromol Res., 18 (2010) 233-240.

[26]. B.D. Cullity, Elements of X-ray Diffraction, Addison-Wesley, Reading, MA, 1978.

[27]. G. Ballerini, K. Ogle, M.G.B. Labrousse, The acid–base properties of the surface of native zinc oxide layers: An XPS study of adsorption of 1,2-diaminoethane, Appl. Surf. Sci. 253 (2007) 6860-6867.

[28]. M.A. Kanjwal, N.A.M. Barakat, F.A. Sheikh, M.S. Khil, H.Y. Kim, Functionalization of Electrospun Titanium Oxide Nanofibers with Silver Nanoparticles: Strongly Effective Photocatalyst, Int. J. Appl. Ceramic. Technol., 7 (2010) E54-E63.

Figure captions

Scheme 1.Illustration showing the formation of nanobranches from nanofibers (1) the colloidal solution after electrospinning forms ZnNP-ZnAc/PVA nanofibers (2). Calcination of these nanofibers results in the formation of ZnO-ZnO nanofibers (3). These nanofibers after specific hydrothermal process develops ZnO nanobranches around ZnO nanofibers (4).

Fig. 1. Low and high magnification SEM images of the dried ZnAc/PVA (A, B) and Zinc powder/ZnAc/PVA nanofibers (C, D).

Fig. 2. Low and high magnification SEM images of the powder obtained after calcination of the ZnAc/PVA nanofiber mats (A, B) and the Zn NPs/ ZnAc/PVA (C, D) at 500 ^{o}C for 90 minutes.

Fig. 3. AFM image and three-dimensional results for the nanofibers obtained from calcination of the ZnAc/PVA (A, C) and Zn NPs/ZnO/PVA (B, D) electrospun nanofiber mats.

Fig. 4. TEM images at high and low magnifications for the nanofibers obtained from calcination of the ZnAc/PVA (A, B) and Zn NPs/ZnAc/PVA nanofiber mats (C, D). The insets in Fig. B and D represent the corresponding SAED patterns.

Fig. 5. SEM image of the pure nanofibers (A, B) and **zinc** powder that contained calcined nanofibers (C, D) as well as the FE-SEM image (E) after the hydrothermal process at 150 ^{o}C for 60 minutes.

Fig. 6. XRD **patterns** for the nanofibers after calcination in the case of Zn NP-free (A) and the hydrothermal product (B).

Fig. 7. TEM images at low and high magnification of the hydrothermally treated nanofibers (A, B) and a high resolution TEM image (HRTEM) of a nanobranch (C): the inset in (C) shows the FFTT pattern.

Fig. 8. **XPS results for the hydrothermally produced nanofibers.**

Fig. 9. Effect of blank, pristine zinc oxide (ZnO) nanofibers and the newly introduced zinc oxide-zinc oxide (ZnO-ZnO) nanostructure on the photocatalytic degradation of methylene blue dye**.**

Table 1. Calculation of crystallite particle size of zinc oxide hierarchical nanostructure from FWHM of X-ray diffraction pattern.

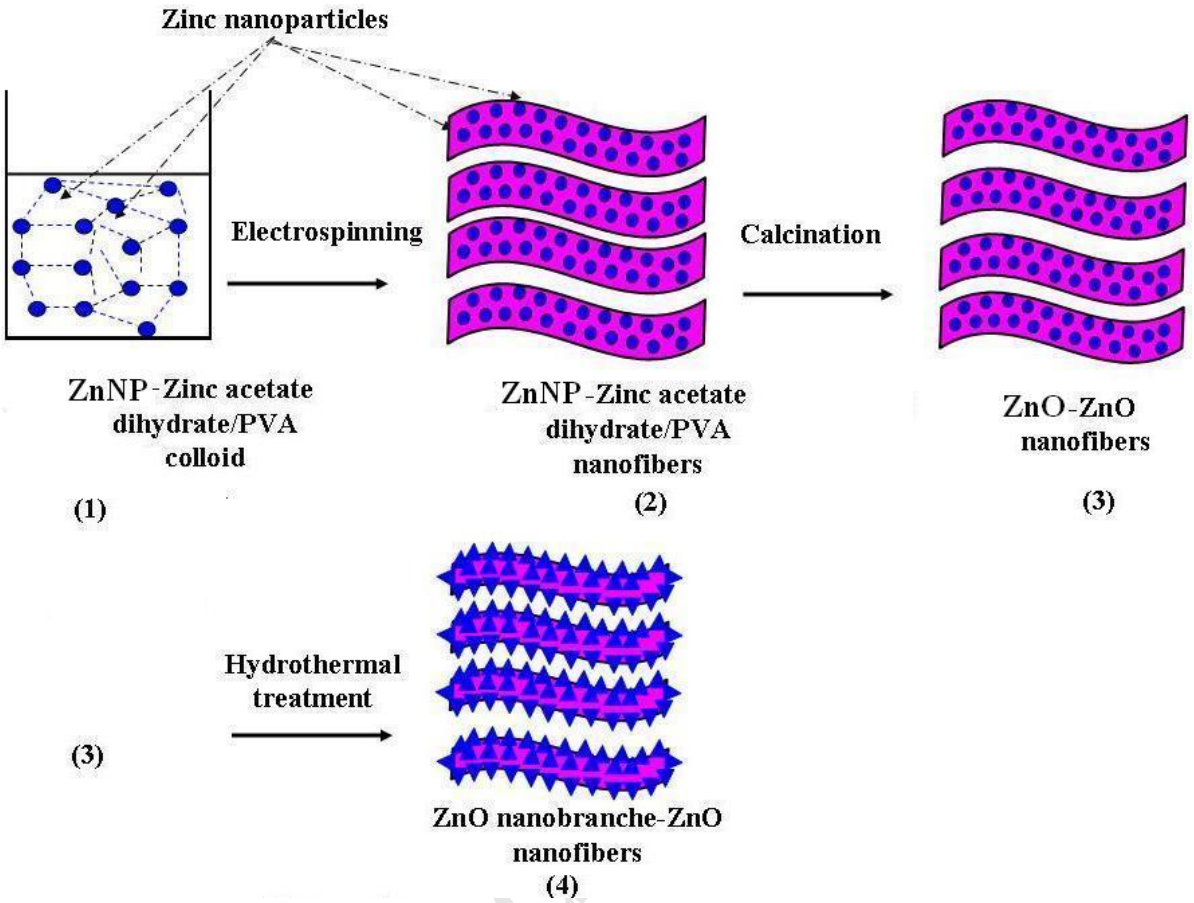

Scheme 1.Illustration showing the formation of nanobranches from nanofibers (1) the colloidal solution after electrospinning forms ZnNP-ZnAc/PVA nanofibers (2). Calcination of these nanofibers results in the formation of ZnO-ZnO nanofibers (3). These nanofibers after specific hydrothermal process develops ZnO nanobranches around ZnO nanofibers (4).

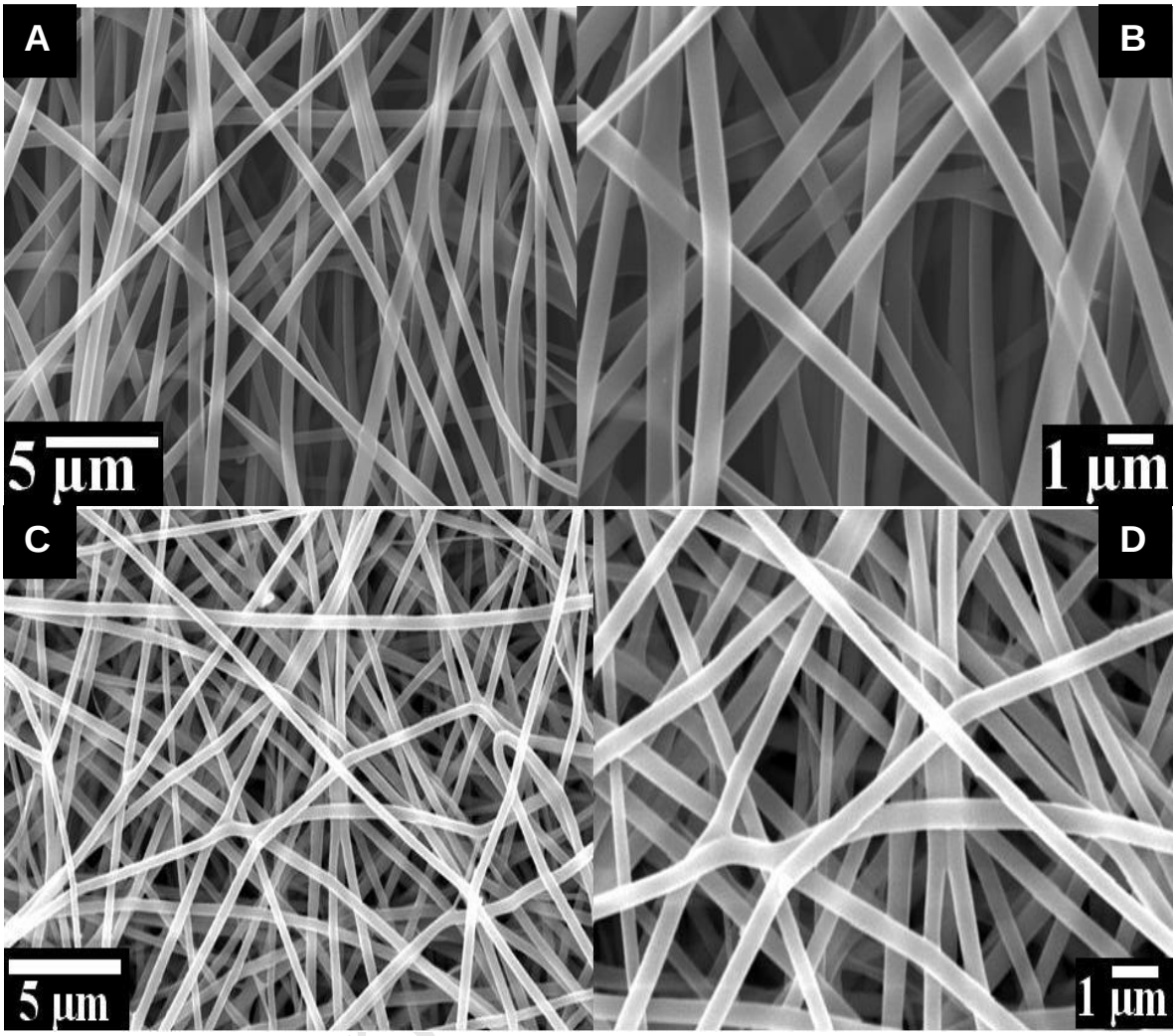

Figure 1. Low and high magnifications SEM images for the dried ZnAc/PVA (A, B), and Zinc powder/ZnAc/PVA nanofibers (C, D).

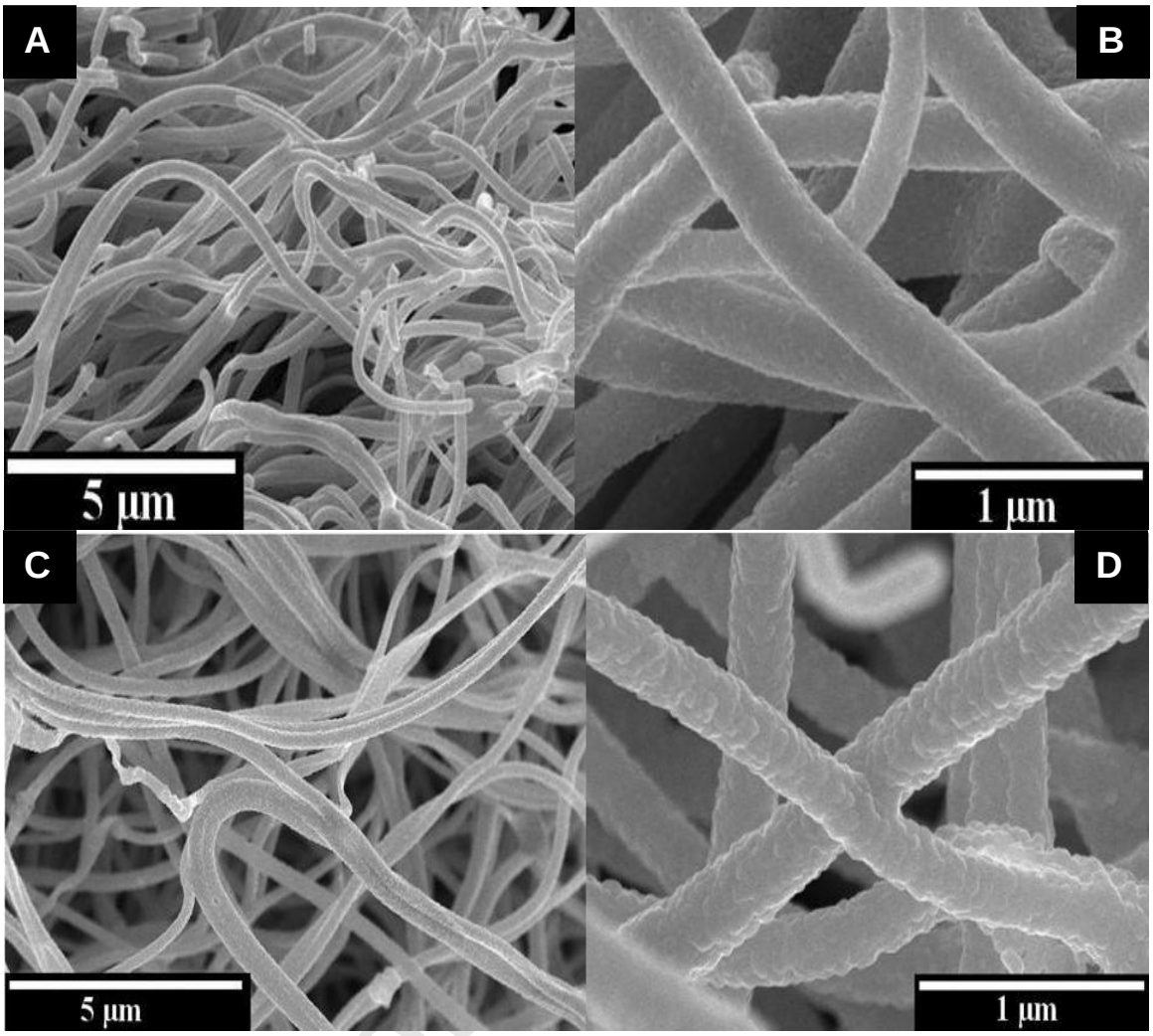

Figure 2. Low and high magnification SEM images of the powder obtained after calcination of the ZnAc/PVA nanofiber mats (A and B), and Zn NPs/ ZnAc/PVA (C and D), at 500 ^{o}C for 90 minutes.

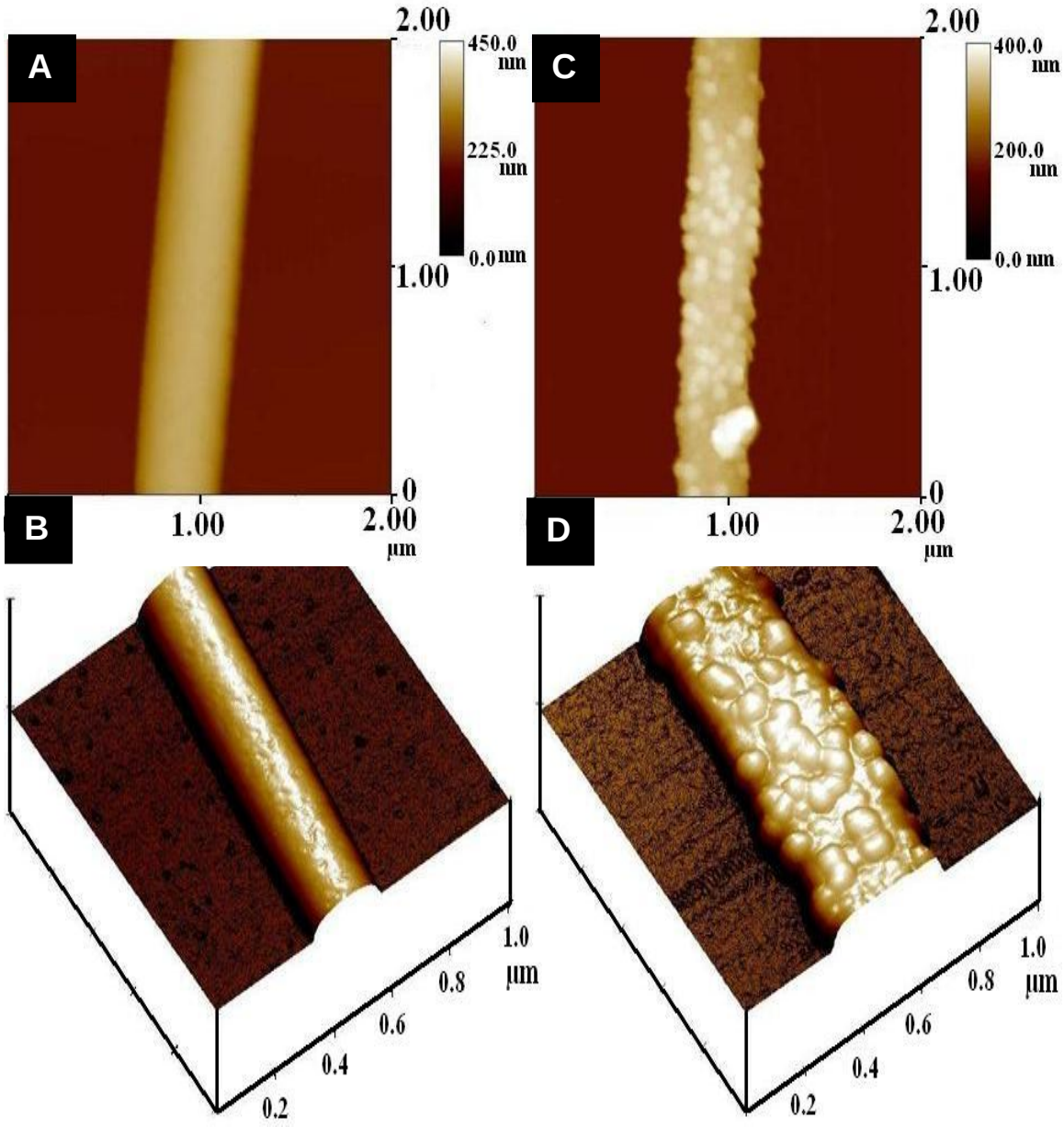

Figure 3. AFM image and three dimensional results for the nanofibers obtained from calcination of ZnAc/PVA (A, C), and Zn NPs/ZnO/PVA (B, D) electrospun nanofiber mats.

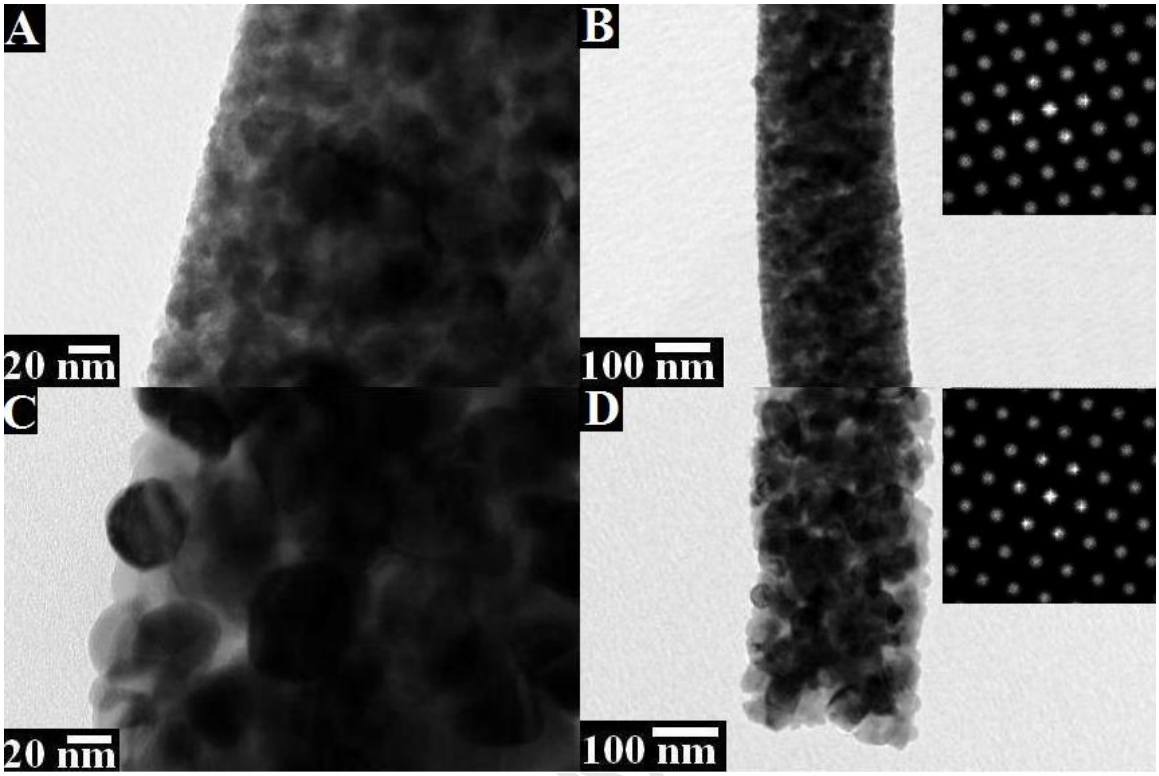

Figure 4. TEM images in high and low magnifications for the nanofibers obtained from calcinations of ZnAc/PVA nanofiber mats; (A, B) and from Zn NPs/ZnAc/PVA nanofiber mats; (C, D). The insets in figures B and D represent the corresponding SAED patterns.

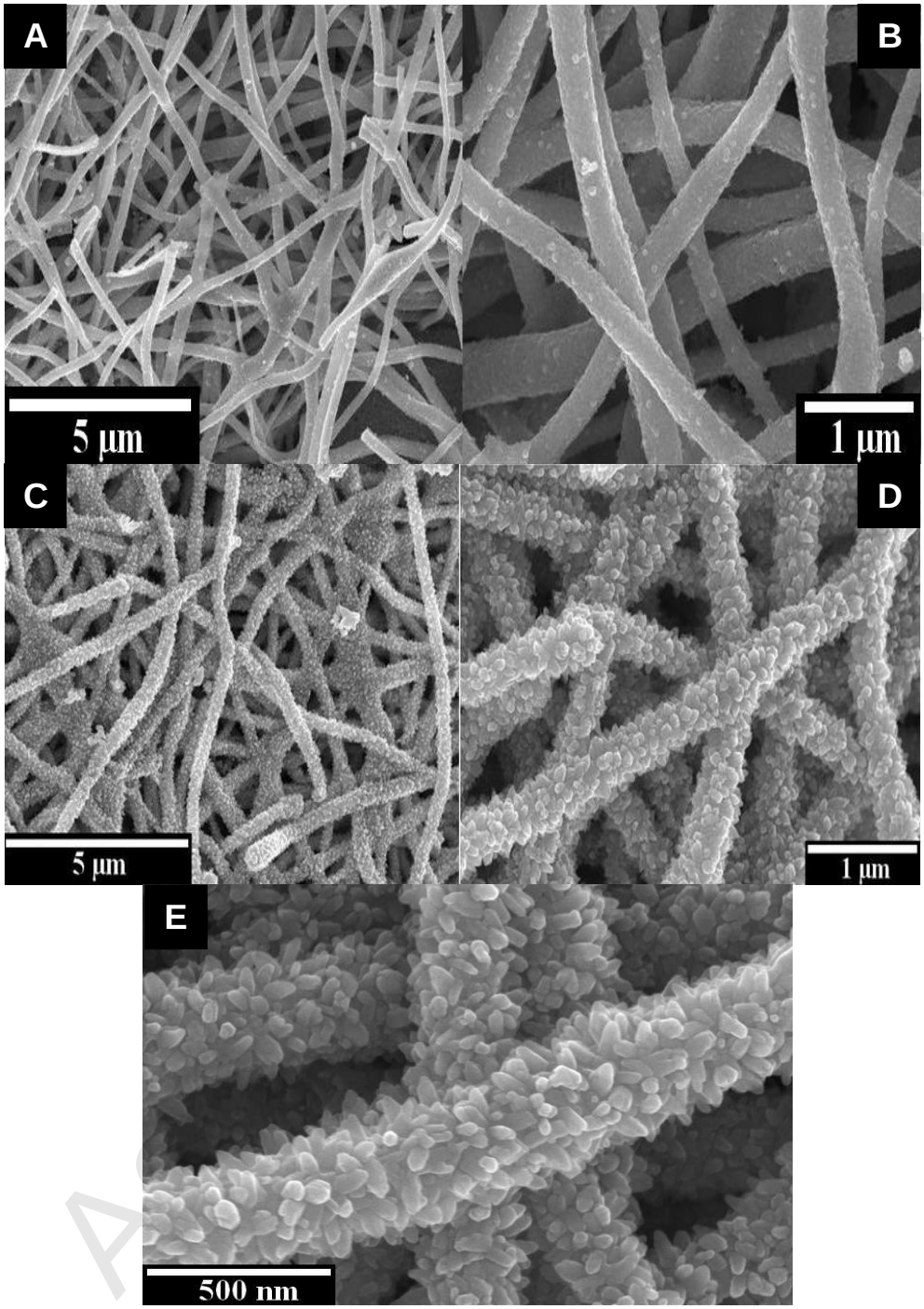

Figure 5. SEM images of the pure nanofibers (A and B) and of **zinc** powder containing calcined nanofibers (C and D) as well as an FE-SEM image (E) after hydrothermal process at 150 ^{o}C for 60 minutes.

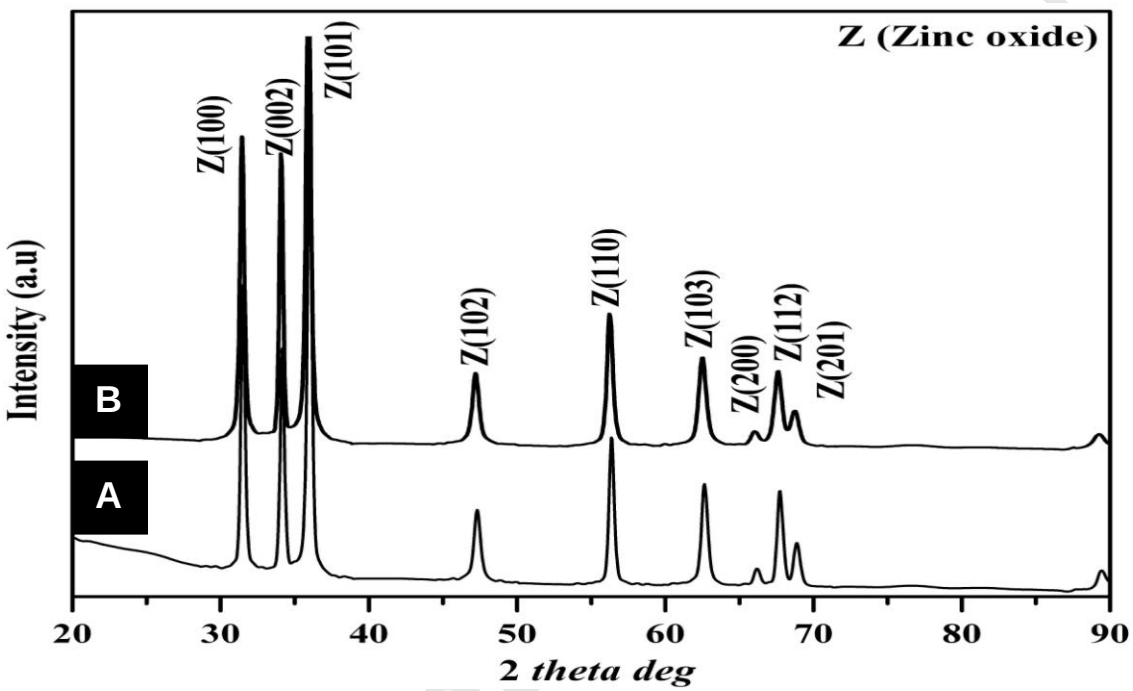

Figure 6. XRD **patterns** for the nanofibers after calcination in the case of Zn NP-free (A) and the hydrothermal product (B).

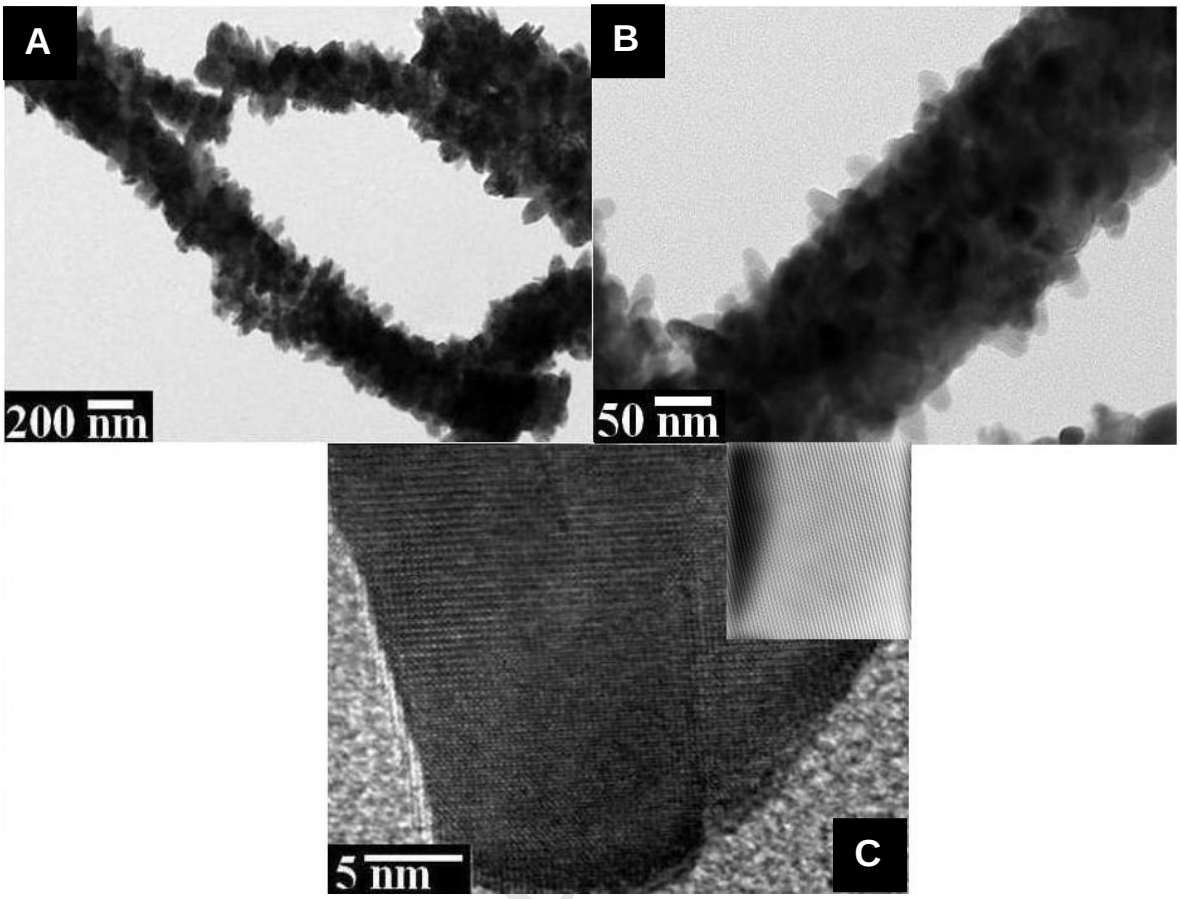

Figure 7. TEM images in low and high magnifications of hydrothermally treated nanofibers (A, B) and a high resolution TEM image (HRTEM) for a nanobranch; the inset in (C) shows the FFTT pattern.

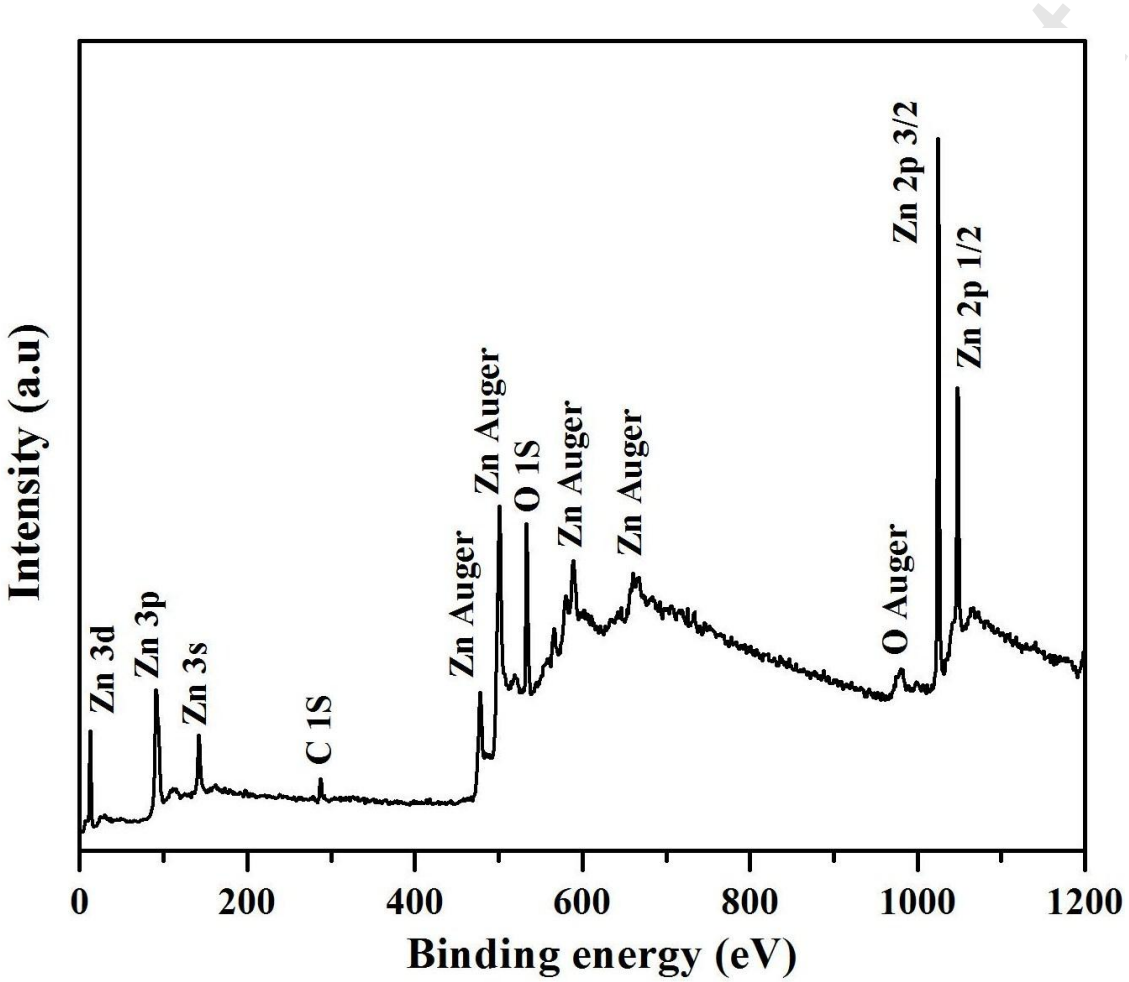

Figure 8. XPS results for the hydrothermally produced nanofibers.

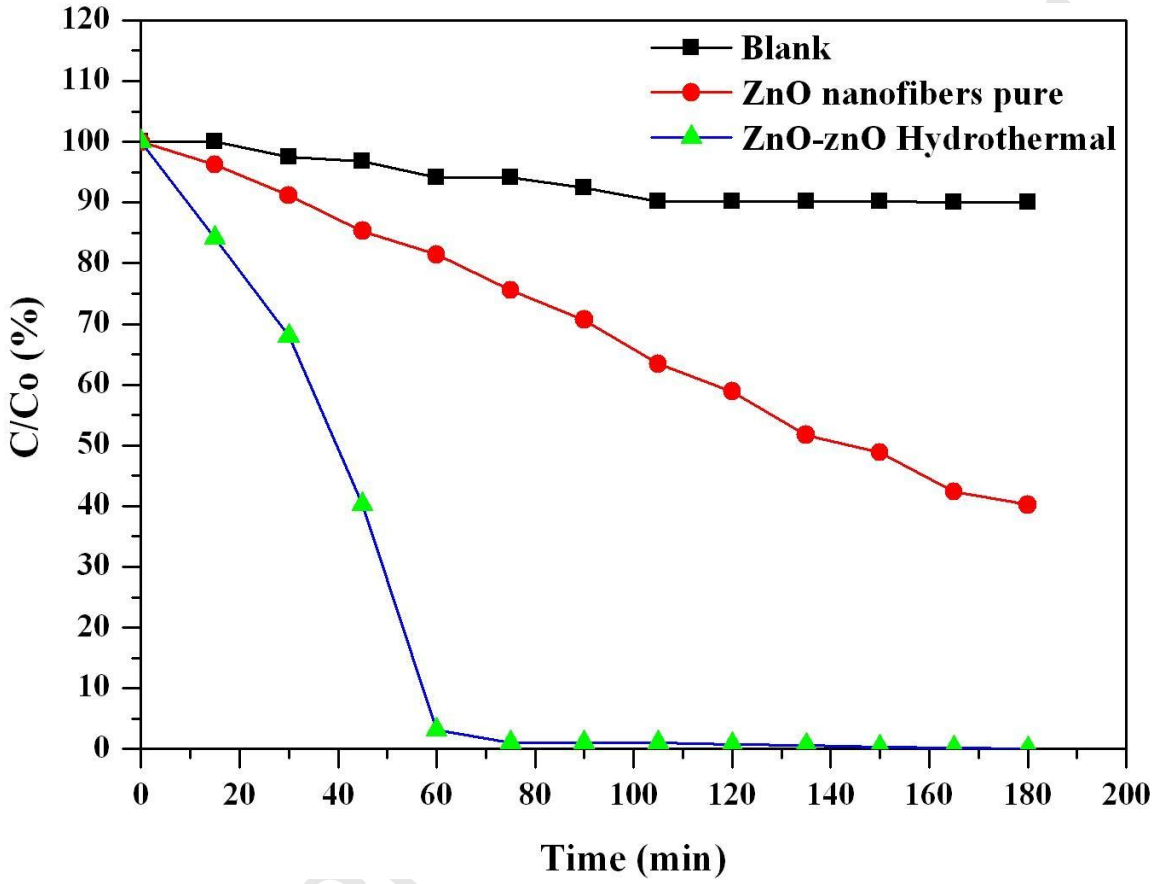

Figure 9. Effect of blank, pristine zinc oxide (ZnO) nanofibers, and the newly introduced zinc oxide-zinc oxide (ZnO-ZnO) nanostructure on the photocatalytic degradation of methylene blue dye.

Table 1

Hydrothermal Product	Phase	Peak position	FWHM (in radian	Cos θ	Particle size (nm)
	100	31.66 ^{o}	0.2204	0.962075296	26.6
	002	34.22 ^{o}	0.3391	0.955741681	32.0
	101	36.25	0.4226	0.950380083	90.8
	102	47.86 ^{o}	0.3857	0.914041698	15.1
	110	56.51 ^{o}	0.5492	0.880890738	19.6
	103	62.66 ^{o}	0.6748	0.854186693	15.9
	200	67.37 ^{o}	0.8763	0.832147749	12.4
	112	67.92 ^{o}	0.8763	0.829427761	12.4
	201	69.26 ^{o}	0.4408	0.822838933	14.3

Calculation of crystallite particle size of zinc oxide hierarchical nanostructure from FWHM of X-ray diffraction pattern.

Figure(s)

Click here to download high resolution image

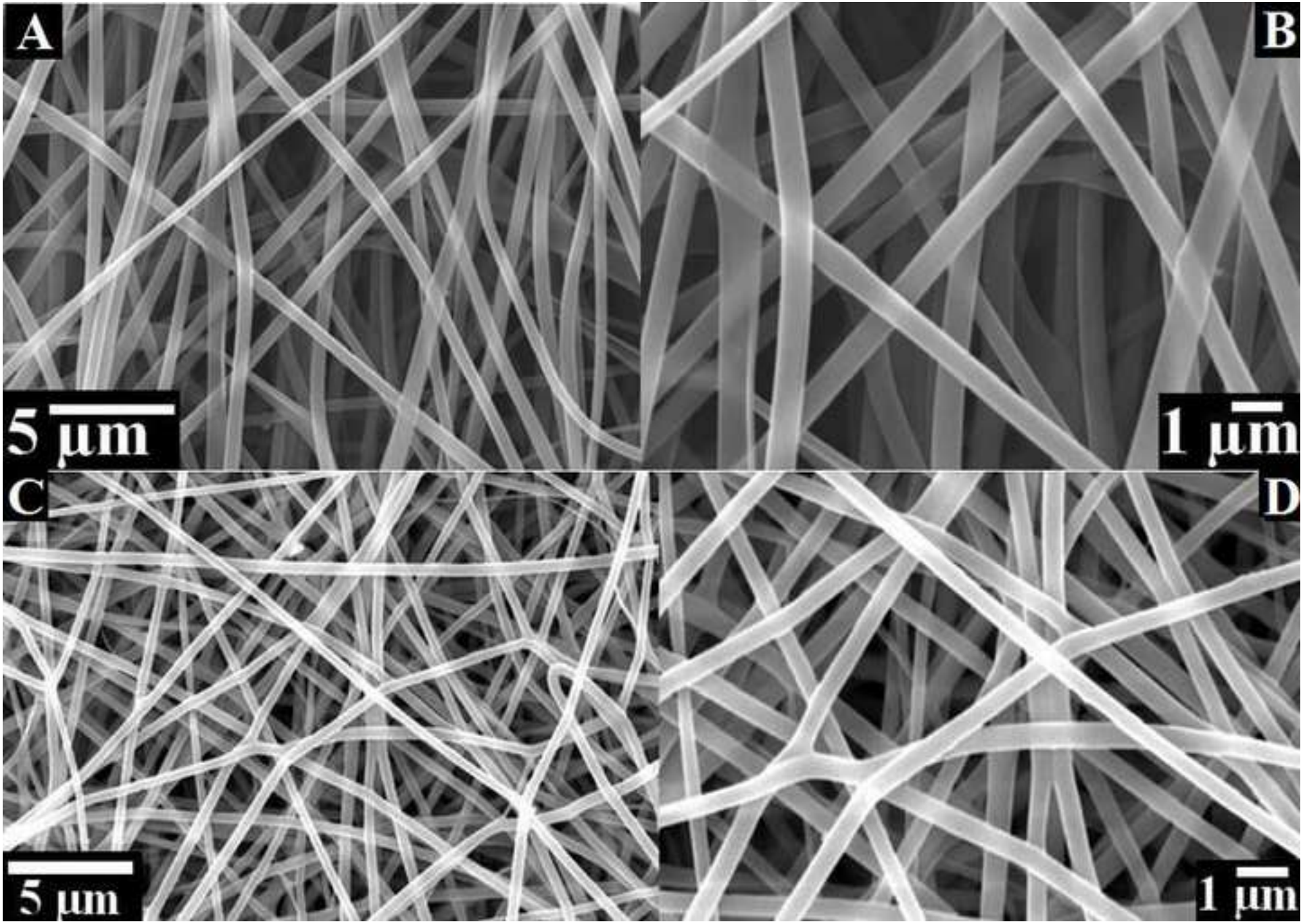

Figure(s)
Click here to download high resolution image

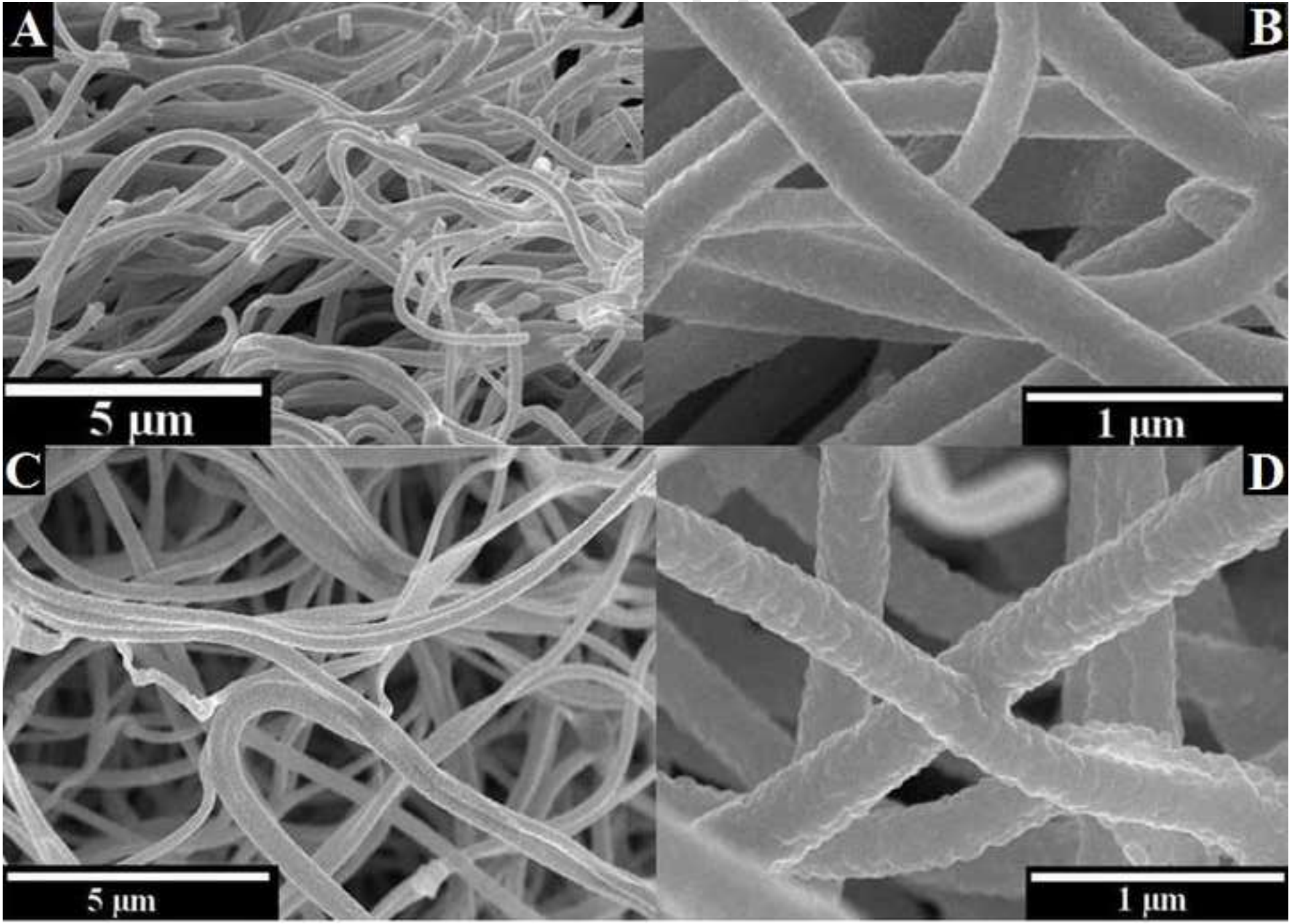

Figure(s)

Click here to download high resolution image

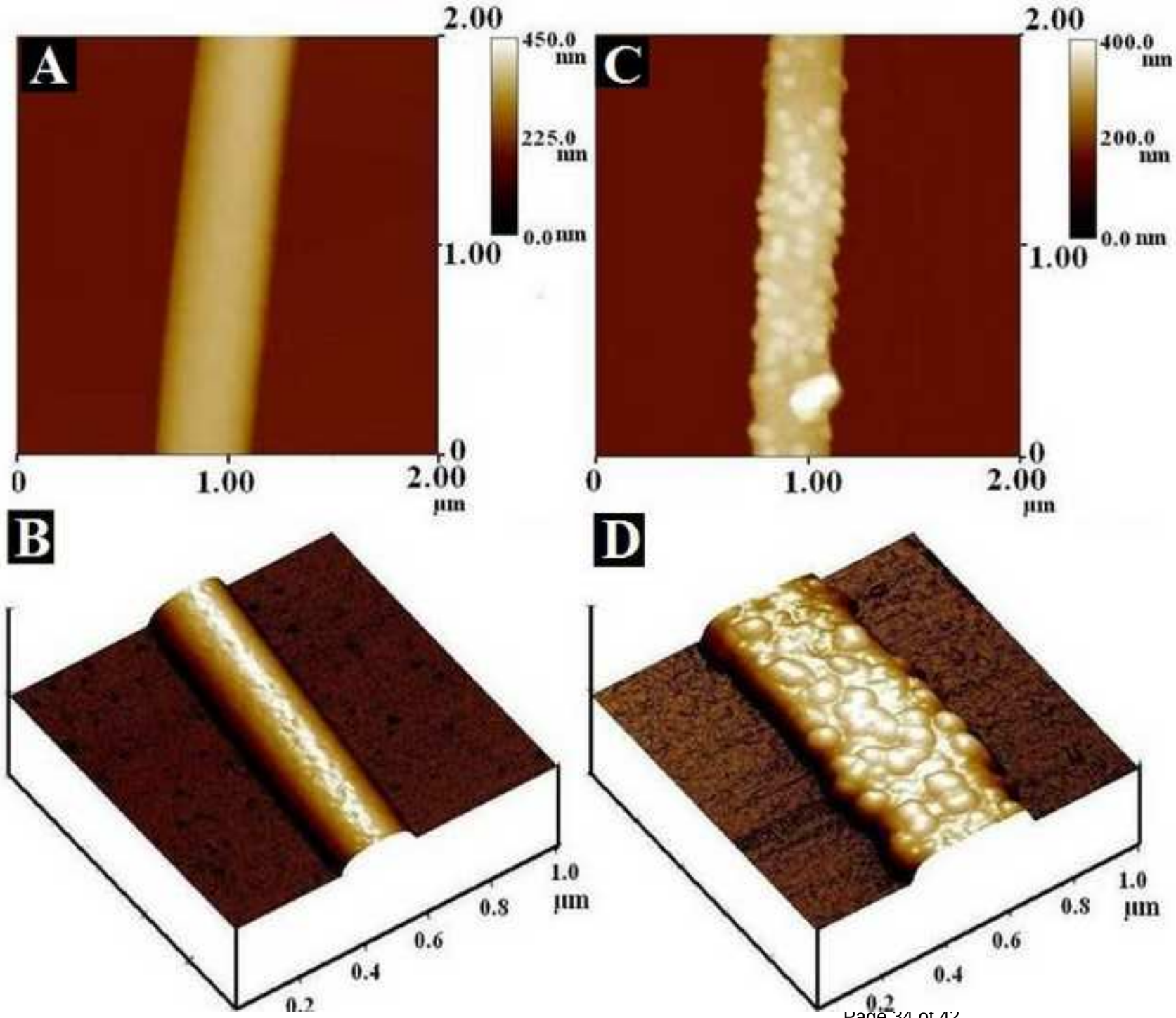

Figure(s)
Click here to download high resolution image

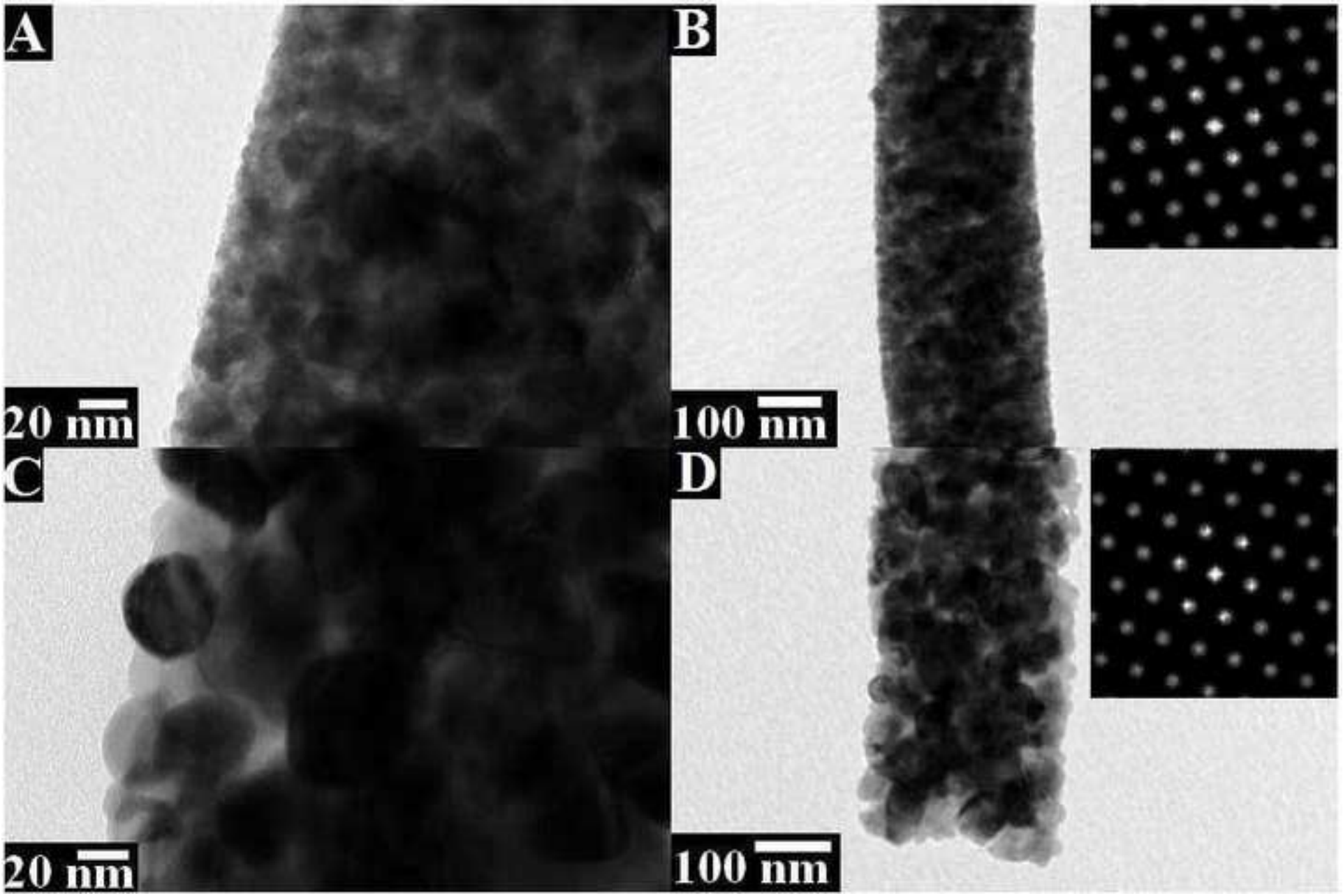

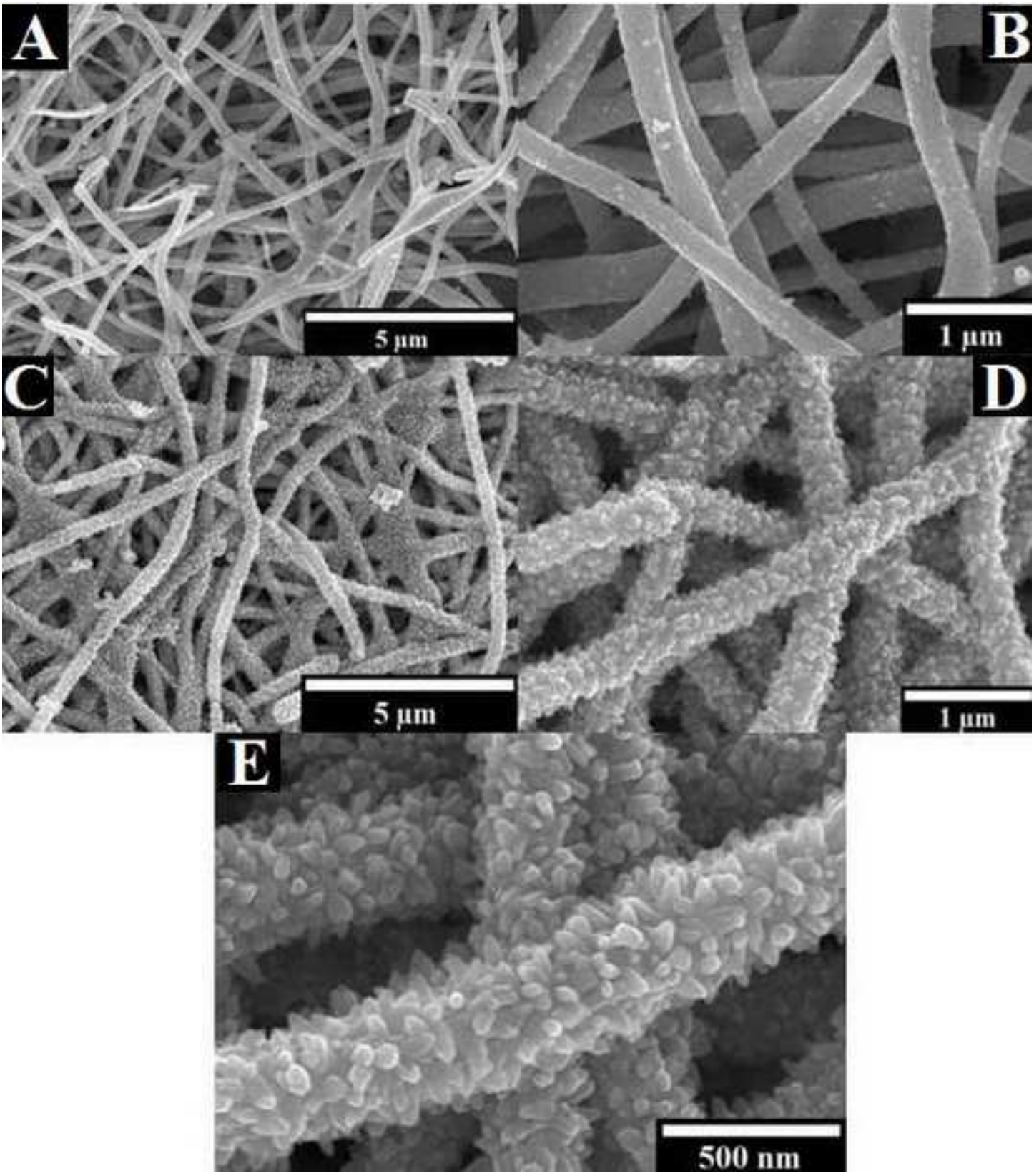

Figure(s)

Click here to download high resolution image

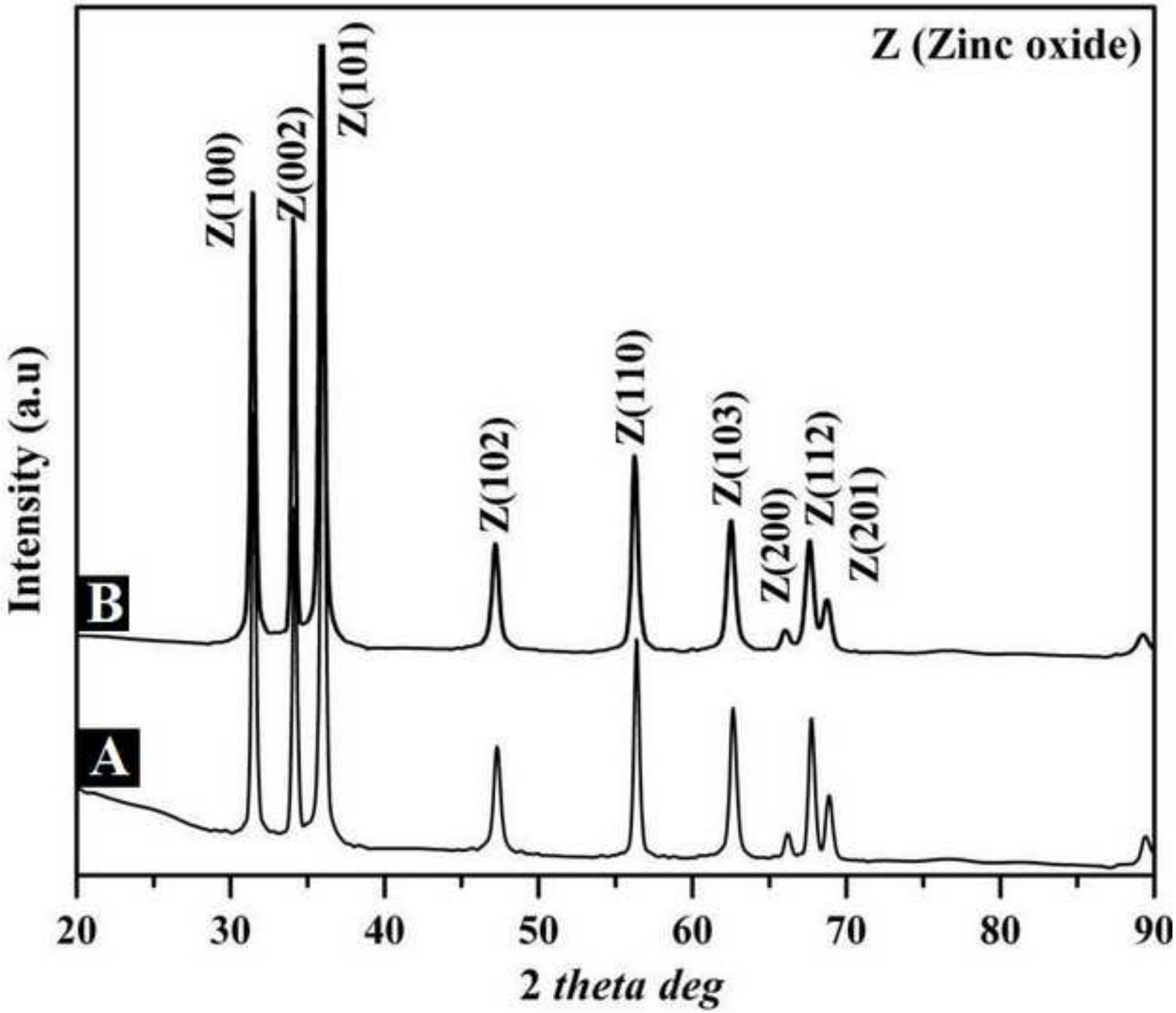

Figure(s)
Click here to download high resolution image

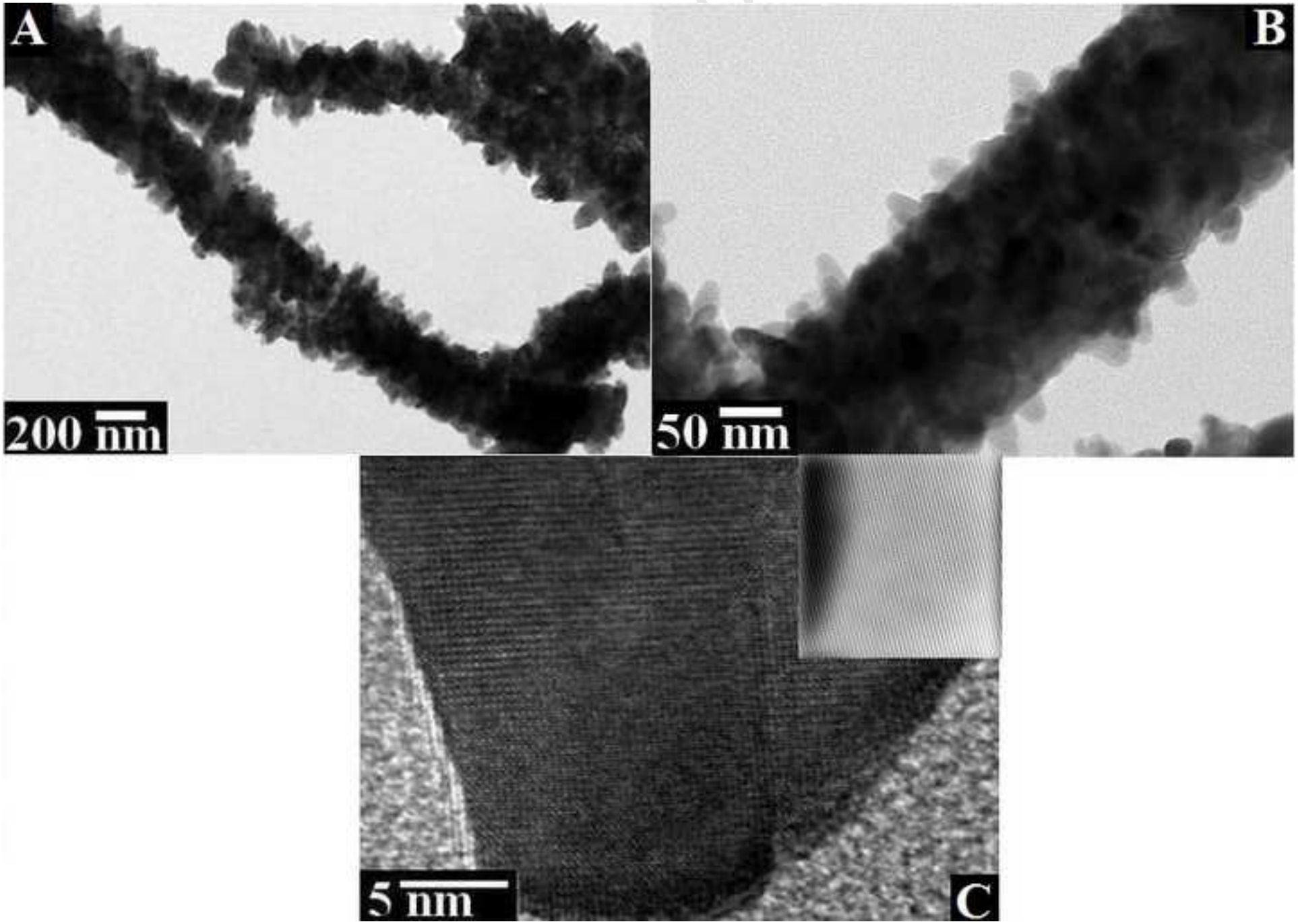

Figure(s)

Click here to download high resolution image

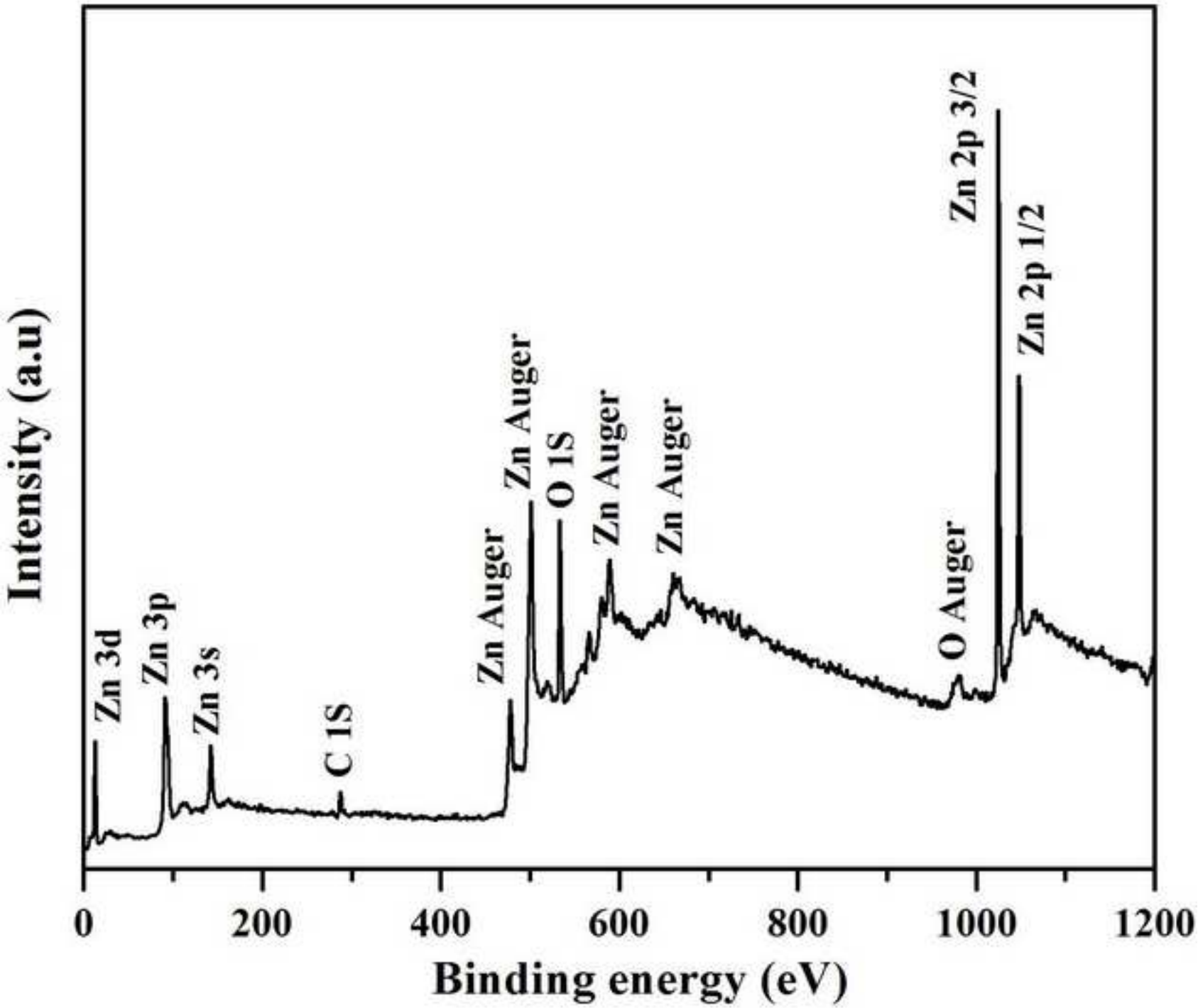

Figure(s)

Click here to download high resolution image

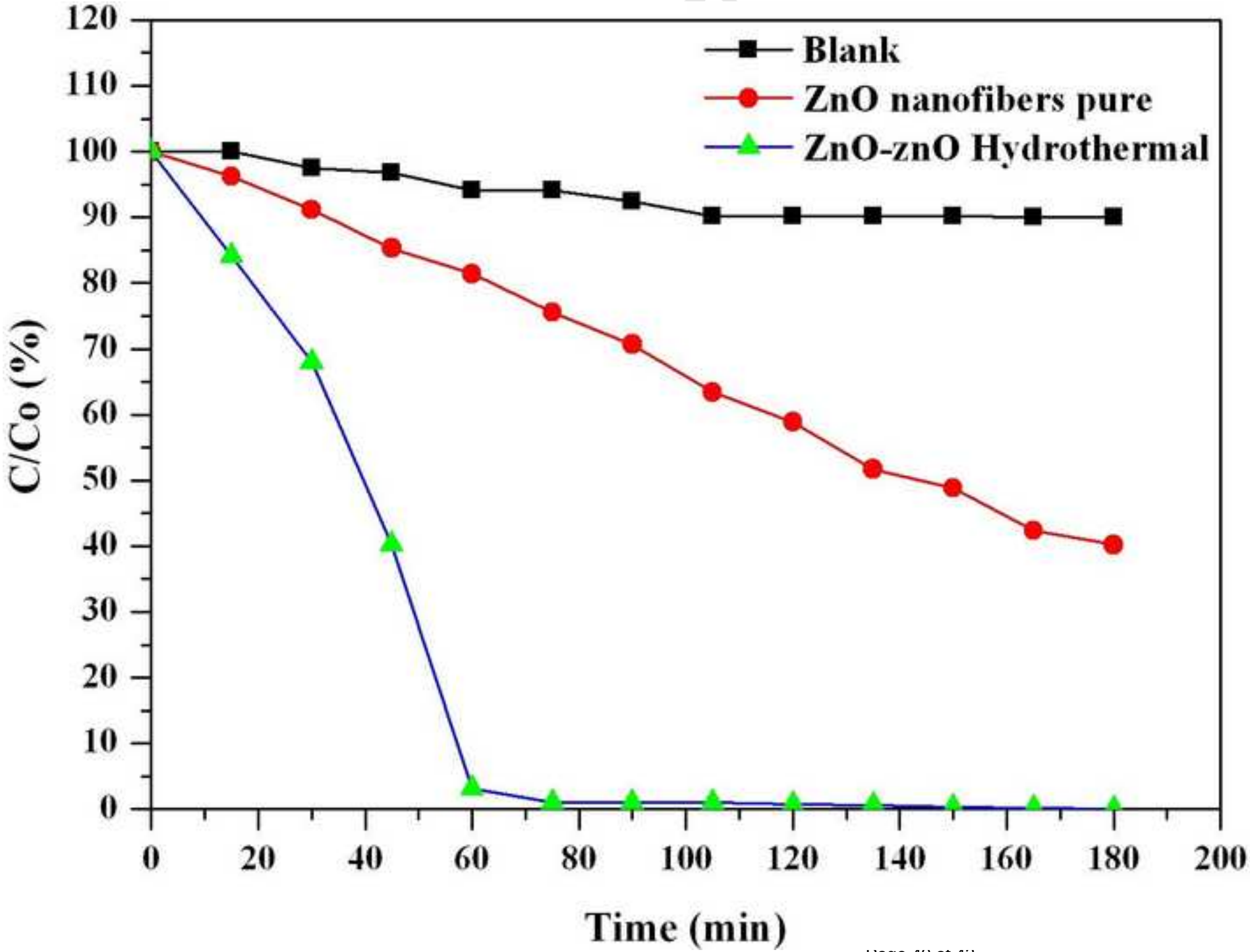

Figure(s)

Click here to download high resolution image

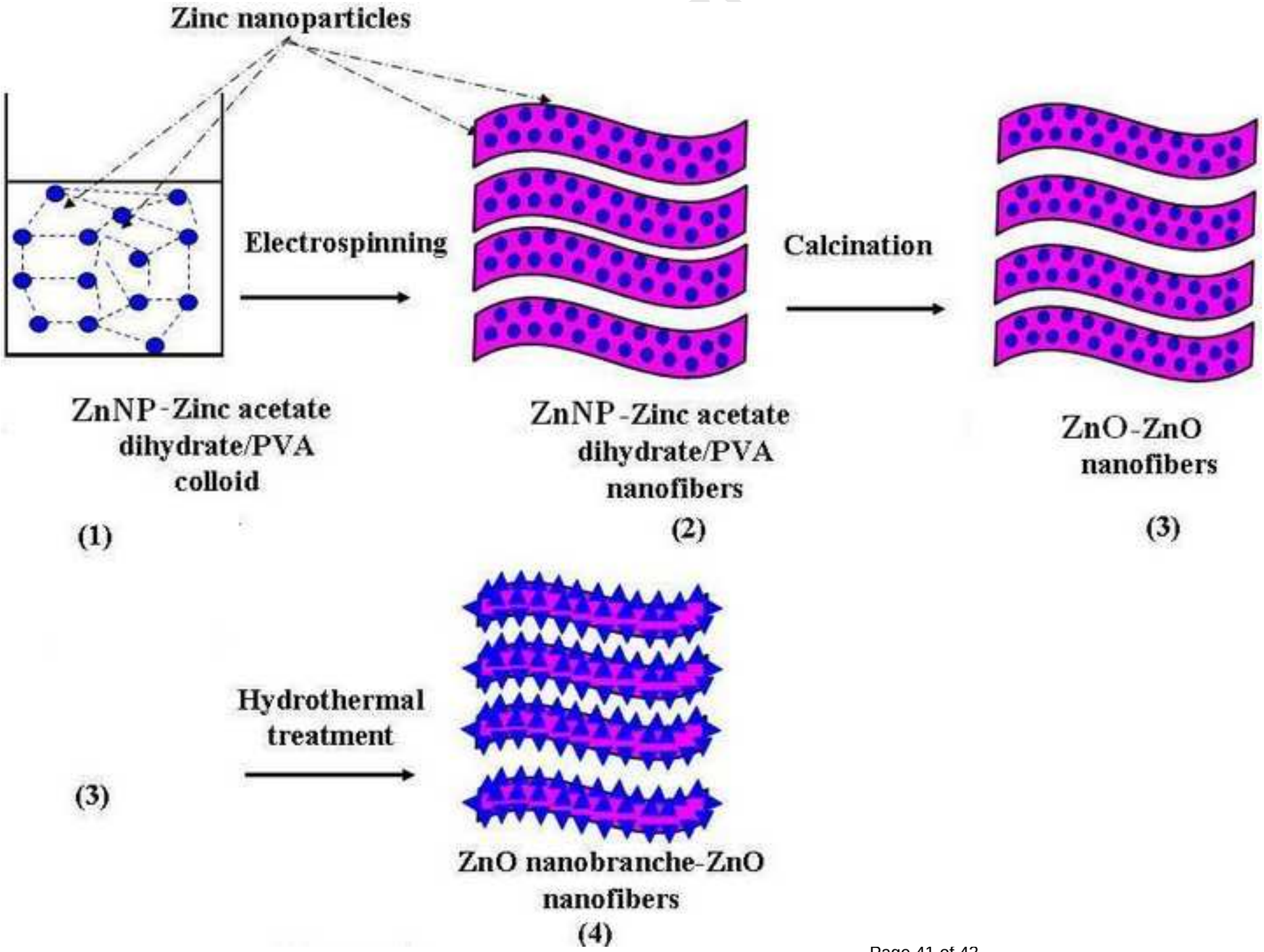

Table(s)
Click here to download high resolution image

Table 1

Calculation of crystallite particle size of zinc oxide hierarchical nanostructure from FWHM of X-ray diffraction pattern.

Hydrothermal Product	Phase	Peak position	FWHM (in radian	Cosθ	Particle size (nm)
	100	31.66°	0.2204	0.962075296	26.6
	002	34.22°	0.3391	0.955741681	32.0
	101	36.25	0.4226	0.950380083	90.8
	102	47.86°	0.3857	0.914041698	15.1
	110	56.51°	0.5492	0.880890738	19.6
	103	62.66°	0.6748	0.854186693	15.9
	200	67.37°	0.8763	0.832147749	12.4
	112	67.92°	0.8763	0.829427761	12.4
	201	69.26°	0.4408	0.822838933	14.3